Loss-of-Function Variants in *CUL3* Cause a Syndromic Neurodevelopmental Disorder

Patrick R. Blackburn, PhD, FACMG,[1] Frédéric Ebstein, PhD,[2,3] Tzung-Chien Hsieh, PhD,[4]
Marialetizia Motta, PhD,[5] Francesca Clementina Radio, MD, PhD,[5]
Johanna C. Herkert, MD, PhD,[6] Tuula Rinne, PhD,[7] Isabelle Thiffault, PhD,[8,9]
Michele Rapp, MS,[10] Mariel Alders, MD, PhD,[11] Saskia Maas, MD,[11]
Bénédicte Gerard, PharmD, PhD,[12] Thomas Smol, MD,[13]
Catherine Vincent-Delorme, MD,[14] Benjamin Cogné, MD,[3,15] Bertrand Isidor, MD,[3,15]
Marie Vincent, MD,[3,15] Ruxandra Bachmann-Gagescu, MD,[16,17] Anita Rauch, MD,[16]
Pascal Joset, PhD,[18] Giovanni Battista Ferrero, MD, PhD,[19] Andrea Ciolfi, PhD,[5]
Thomas Husson, MD, PhD,[20,21] Anne-Marie Guerrot, MD,[21] Carlos Bacino, MD, FACMG,[22]
Colleen Macmurdo, DO,[23] Stephanie S. Thompson, MS, CGC,[23]
Jill A. Rosenfeld, MS, CGC,[22,24] Laurence Faivre, MD, PhD,[25,26]
Frederic Tran Mau-Them, MD, PhD,[26,27] Wallid Deb, BSc,[3,15] Virginie Vignard, MS,[3,15]
Pankaj B. Agrawal, MD, MMSc,[28,29] Jill A. Madden, PhD, MSc, CGC,[28,29]
Alice Goldenberg, MD,[21] François Lecoquierre, MD,[21] Michael Zech, MD,[30,31,32]
Holger Prokisch, PhD ⬤,[30,31,32] Ján Necpál, MD,[33,34] Robert Jech, MD, PhD,[35]
Juliane Winkelmann, MD,[36,37,38,39] Monika Turčanová Koprušáková, MD, PhD,[40]
Vassiliki Konstantopoulou, MD,[41] John R. Younce, MD,[42]
Marwan Shinawi, MD, FACMG ⬤,[43,44] Chloe Mighton, MSc,[45,46]
Charlotte Fung, MSc, CGC,[47,48] Chantal F. Morel, BSc, MD, FRCPC,[47,49]
Jordan Lerner-Ellis, PhD, FACMG,[50,51,52] Stephanie DiTroia, PhD,[53]
Magalie Barth, MD,[54,55] Dominique Bonneau, MD, PhD,[54] Ingrid Krapels, MD, PhD,[56,57]
Alexander P.A. Stegmann, PhD,[56,57] Vyne van der Schoot, MD, PhD,[56,57]
Theresa Brunet, MD ⬤,[58,59] Cornelia Bußmann, MD,[60] Cyril Mignot, MD, PhD,[61]
Giuseppe Zampino, MD,[62,63] Saskia B. Wortmann, MD, PhD,[64] Johannes A. Mayr, MD,[64]
René G. Feichtinger, PhD,[64] Thomas Courtin, MD,[65] Claudia Ravelli, MD,[66]
Boris Keren, MD, PhD,[61] Alban Ziegler, MD,[55,67] Linda Hasadsri, MD, PhD,[68]
Pavel N. Pichurin, MD,[69] Eric W. Klee, PhD,[69,70,71] Katheryn Grand, MS, CGC,[72]
Pedro A. Sanchez-Lara, MD, MSCE, FAAP, FACMG,[72] Elke Krüger, PhD,[2]
Stéphane Bézieau, PharmD, PhD,[3,15] Hannah Klinkhammer, MSc,[4,73]

ANNALS *of Neurology*

Peter Michael Krawitz, MD, PhD,[4] Evan E. Eichler, PhD,[74,75] Marco Tartaglia, PhD [ID],[5]
Sébastien Küry, DVM, PhD,[3,15] and Tianyun Wang, PhD [ID][76,77,78,79]

Objective: De novo variants in *cullin-3 ubiquitin ligase* (*CUL3*) have been strongly associated with neurodevelopmental disorders (NDDs), but no large case series have been reported so far. Here, we aimed to collect sporadic cases carrying

From the [1]Department of Pathology, St. Jude Children's Research Hospital, Memphis, TN, USA; [2]Institute of Medical Biochemistry and Molecular Biology, University Medicine Greifswald, Greifswald, Germany; [3]Nantes Université, CHU Nantes, CNRS, INSERM, l'institut du Thorax, Nantes, France; [4]Institute of Genomic Statistics and Bioinformatics, University of Bonn, Bonn, Germany; [5]Molecular Genetics and Functional Genomics, Ospedale Pediatrico Bambino Gesù, IRCCS, Rome, Italy; [6]Department of Genetics, University of Groningen, University Medical Center Groningen, Groningen, The Netherlands; [7]Department of Human Genetics, Radboud University Medical Center, Nijmegen, The Netherlands; [8]Center for Pediatric Genomic Medicine, Children's Mercy Hospital, Kansas City, MO, USA; [9]Department of Pathology and Laboratory Medicine, Children's Mercy Hospitals, Kansas City, MO, USA; [10]Department of Pediatrics-Clinical Genetics and Metabolism, Children's Hospital Colorado, Aurora, CO, USA; [11]Amsterdam University Medical Center, University of Amsterdam, Department of Clinical Genetics, Amsterdam, The Netherlands; [12]Unité de Biologie et de Génétique Moléculaire, Center Hospitalier Universitaire de Strasbourg, Strasbourg, France; [13]Univ Lille, CHU Lille, RADEME Team, Institut de Génétique Médicale, Lille, France; [14]Department of Clinical Genetics, Hôpital Jeanne de Flandre, CHU Lille, Lille, France; [15]Nantes Université, CHU de Nantes, Service de Génétique Médicale, Nantes, France; [16]Institute of Medical Genetics, University of Zurich, Schlieren, Switzerland; [17]Department of Molecular Life Sciences, University of Zurich, Zurich, Switzerland; [18]Medical Genetics, Institute of Medical Genetics and Pathology, University Hospital Basel, Basel, Switzerland; [19]Department of Clinical and Biological Sciences, San Luigi Gonzaga University Hospital, University of Torino, Turin, Italy; [20]Department of Research, Center Hospitalier du Rouvray, Rouen, France; [21]Normandie Univ, UNIROUEN, Inserm U1245 and CHU Rouen, Department of Genetics and Reference Center for Developmental Disorders, Rouen, France; [22]Department of Molecular and Human Genetics, Baylor College of Medicine, Houston, TX, USA; [23]Division of Medical Genetics, Department of Internal Medicine, Baylor Scott and White Medical Center, Temple, TX, USA; [24]Baylor Genetics, Houston, TX, USA; [25]Centre de Génétique et Centre de Référence Anomalies du Développement et Syndromes Malformatifs, FHU TRANSLAD CHU, Dijon, France; [26]INSERM UMR1231, équipe GAD, Université de Bourgogne-Franche Comté, Dijon, France; [27]Unité Fonctionnelle Innovation en Diagnostic Génomique des Maladies Rares, FHU-TRANSLAD, CHU Dijon Bourgogne, Dijon, France; [28]Division of Genetics and Genomics, The Manton Center for Orphan Disease Research, Boston, MA, USA; [29]Division of Neonatology, Department of Pediatrics, University of Miami Miller School of Medicine and Holtz Children's Hospital, Jackson Health System, Miami, FL, USA; [30]Institute of Neurogenomics, Helmholtz Zentrum München, Munich, Germany; [31]Institute of Human Genetics, School of Medicine, Technical University of Munich, Munich, Germany; [32]Institute for Advanced Study, Technical University of Munich, Garching, Germany; [33]Department of Neurology, Zvolen Hospital, Zvolen, Slovakia; [34]Department of Neurology, Faculty of Medicine, Comenius University, Bratislava, Slovakia; [35]Department of Neurology, Charles University, First Faculty of Medicine and General University Hospital, Prague, Czech Republic; [36]Institute of Neurogenomics, Helmholtz Zentrum Muenchen, Neuherberg, Germany; [37]Neurogenetics, Technische Universitaet Muenchen, Munich, Germany; [38]Institute of Human Genetics, Klinikum rechts der Isar der TUM, Munich, Germany; [39]Munich Cluster for Systems Neurology (SyNergy), Munich, Germany; [40]Jessenius Faculty of Medicine in Martin, Comenius University Bratislava, Martin, Slovakia; [41]Department of Pediatrics and Adolescent Medicine, Medical University of Vienna, Vienna, Austria; [42]Department of Neurology, University of North Carolina at Chapel Hill, Chapel Hill, NC, USA; [43]Division of Genetics and Genomic Medicine, St. Louis Children's Hospital, St. Louis, MO, USA; [44]Department of Neurology, Washington University School of Medicine, St. Louis, MO, USA; [45]Institute of Health Policy, Management and Evaluation, University of Toronto, Toronto, Canada; [46]Genomics Health Services and Policy Research Program, Li Ka Shing Knowledge Institute, St. Michael's Hospital, Unity Health Toronto, Toronto, Canada; [47]The Fred A. Litwin Family Centre in Genetic Medicine, University Health Network and Sinai Health System, Toronto, Canada; [48]Department of Molecular Genetics, University of Toronto, Toronto, Canada; [49]Department of Medicine, University of Toronto, Toronto, Canada; [50]Pathology and Laboratory Medicine, Mount Sinai Hospital, Sinai Health, Toronto, Canada; [51]Laboratory Medicine and Pathobiology, University of Toronto, Toronto, Canada; [52]Lunenfeld-Tanenbaum Research Institute, Sinai Health, Toronto, Canada; [53]Center for Mendelian Genomics, Program in Medical and Population Genetics, Broad Institute of MIT and Harvard, Cambridge, MA, USA; [54]Department of Biochemistry and Genetics, University Hospital of Angers, Angers, France; [55]Mitovasc Unit, UMR CNRS 6015-INSERM 1083, Angers, France; [56]Department of Clinical Genetics, Maastricht University Medical Center, Maastricht, The Netherlands; [57]Department of Clinical Genetics and School for Oncology and Developmental Biology, Maastricht UMC, Maastricht, The Netherlands; [58]Institute of Human Genetics, Klinikum rechts der Isar, School of Medicine, Technical University of Munich, Munich, Germany; [59]Dr. v. Hauner Children's Hospital, Department of Pediatric Neurology and Developmental Medicine, LMU—University of Munich, Munich, Germany; [60]Department of Neuropediatrics, ATOS Klinik Heidelberg, Heidelberg, Germany; [61]Département de Génétique, AP-HP-Sorbonne Université, Hôpital Trousseau & Groupe Hospitalier Pitié-Salpêtrière, Paris, France; [62]Center for Rare Diseases and Birth Defects, Department of Woman and Child Health and Public Health, Fondazione Policlinico Universitario A. Gemelli IRCCS, Rome, Italy; [63]Dipartimento di Scienze Della Vita e Sanità Pubblica, Università Cattolica del Sacro Cuore, Rome, Italy; [64]University Children's Hospital, Paracelsus Medical University (PMU), Salzburg, Austria; [65]Center for Molecular and Chromosomal Genetics, AP-HP-Sorbonne University, Pitié-Salpêtrière Hospital, Paris, France; [66]Department of Pediatric Neurology and Neurogenetic Referral Center, AP-HP-Sorbonne Université, Armand Trousseau Hospital, Paris, France; [67]Department of Biochemistry and Genetics, Angers University Hospital and UMR CNRS, Angers, France; [68]Division of Laboratory Genetics and Genomics, Department of Laboratory Medicine and Pathology, Mayo Clinic, Rochester, MN, USA; [69]Department of Clinical Genomics, Mayo Clinic, Rochester, MN, USA; [70]Department of Quantitative Health Sciences Research, Mayo Clinic, Rochester, MN, USA; [71]Center for Individualized Medicine, Mayo Clinic, Rochester, MN, USA; [72]Department of Pediatrics, Guerin Children's at Cedars-Sinai Medical Center, Los Angeles, CA, USA; [73]Institute of Medical Biometry, Informatics and Epidemiology, University of Bonn, Bonn, Germany; [74]Department of Genome Sciences, University of Washington School of Medicine, Seattle, WA, USA; [75]Howard Hughes Medical Institute, University of Washington, Seattle, WA, USA; [76]Department of Medical Genetics, Center for Medical Genetics, School of Basic Medical Sciences, Peking University, Beijing, China; [77]Neuroscience Research Institute, Peking University, Beijing, China; [78]Key Laboratory for Neuroscience, Ministry of Education of China & National Health Commission of China, Beijing, China; and [79]Autism Research Center, Peking University Health Science Center, Beijing, China

Additional supporting information can be found in the online version of this article.

rare variants in *CUL3*, describe the genotype–phenotype correlation, and investigate the underlying pathogenic mechanism.

Methods: Genetic data and detailed clinical records were collected via multicenter collaboration. Dysmorphic facial features were analyzed using GestaltMatcher. Variant effects on CUL3 protein stability were assessed using patient-derived T-cells.

Results: We assembled a cohort of 37 individuals with heterozygous *CUL3* variants presenting a syndromic NDD characterized by intellectual disability with or without autistic features. Of these, 35 have loss-of-function (LoF) and 2 have missense variants. *CUL3* LoF variants in patients may affect protein stability leading to perturbations in protein homeostasis, as evidenced by decreased ubiquitin-protein conjugates in vitro. Notably, we show that 4E-BP1 (EIF4EBP1), a prominent substrate of CUL3, fails to be targeted for proteasomal degradation in patient-derived cells.

Interpretation: Our study further refines the clinical and mutational spectrum of *CUL3*-associated NDDs, expands the spectrum of cullin RING E3 ligase-associated neuropsychiatric disorders, and suggests haploinsufficiency via LoF variants is the predominant pathogenic mechanism.

Cullin 3 (aka CUL3 or PHA2E) is an evolutionarily conserved component of the CUL3-RING E3 ubiquitin ligase (CRL) complex, which together mediate the selective ubiquitination and subsequent proteasomal degradation of a variety of target proteins.[1,2] The cullin-RING ligases (CRLs) include 8 known highly conserved cullin protein members: CUL1, CUL2, CUL3, CUL4A, CUL4B, CUL5, CUL7, and CUL9.[1] Germline variants in several of the genes encoding these proteins have been associated with syndromic disorders, namely Cabezas type of X-linked syndromic intellectual disability (ID) (MRXSC, OMIM 300354) caused by hemizygous *CUL4B* variants,[3,4] and 3-M syndrome 1 (3M1, OMIM 273750) caused by biallelic *CUL7* variants.[5]

Heterozygous, predominantly *de novo*, gain-of-function variants affecting splicing of exon 9 in *CUL3* cause autosomal dominant pseudohypoaldosteronism type IIE (PHA2E, OMIM 614496), which presents with hyperkalemia and hyperchloremia with hyperchloremic metabolic acidosis leading to early-onset hypertension.[6] Individual reports and small cohorts have identified several patients with *de novo* loss-of-function (LoF) variants, including splice site, stop-gain variants, and missense variants, who presented with a variety of clinical phenotypes including neurodevelopmental disorder (NDD), autism spectrum disorder (ASD), and global developmental delays with or without infantile spasms.[7–10] LoF variants in *CUL3* have also been reported in several large cohorts of patients with congenital heart defects, suggesting it may also have a broader role in early development, however, NDDs were either not evaluated or described in patients in these studies.[11] Trio-based exome sequencing studies in families with sporadic cases of ASD have uncovered *de novo CUL3* variants in affected children (OMIM 619239).[12–14] Recently, *CUL3* was also found to be associated with an increased risk of ASD in large genome-wide association studies.[15,16]

Although *CUL3* is ubiquitously expressed in the brain, its role in the central nervous system is still poorly understood. Studies in mice have shown that the association of potassium channel tetramerization domain containing 13 (Kctd13) with Cul3 mediates the ubiquitination of Ras homolog family member A (RhoA), affecting the actin cytoskeleton, synaptic transmission, and potentially influencing brain development.[17] ASD-associated nonsense *CUL3* variants have been reported to disrupt the physical interaction between KCTD13 and CUL3, which may suggest a possible pathogenic mechanism for *CUL3* haploinsufficiency.[17]

Changes in neuronal migration and lamination defects have been linked to ASD in humans and mice, implicating *CUL3* haploinsufficiency in ASD-related neurobehavioral abnormalities. Studies in $Cul3^{+/-}$ mice showed social and behavioral abnormalities with increased anxiety levels, altered synaptic dynamics, and disrupted excitation-inhibition (E-I) balance in CA1 and pyramidal neurons.[18] *Cul3* haploinsufficiency resulted in increased levels of Eif4g1, a protein involved in translational homeostasis, and upregulated Cap-dependent protein synthesis in the brains of mice, which may underlie the neurodevelopmental and neuropsychological deficits.[18] Another study showed Cul3 is an important regulator of neuronal migration during early mouse development, with $Cul3^{+/-}$ mice developing cortical lamination abnormalities resulting in motor and behavioral deficits.[19] Loss of *Cul3* led to upregulation of proteins including plastin3 (Pls3), which regulates actin organization and cell migration speed, potentially disrupting cytoskeletal organization and protein homeostasis during a critical developmental window, leading to observed cortical changes in $Cul3^{+/-}$ mice.[19] Interestingly, they did not see elevation of RhoA in embryonic forebrain tissue from $Cul3^{+/-}$ mice in their study.[19]

In this study, we describe a cohort of 37 patients, the largest to our knowledge, with *CUL3*-associated syndromic ID with autistic features. Through meta-analysis in large ASD and developmental delay (DD) trio-exome

cohorts (n = 46247), functional studies using patient derived cells, and facial profiling, we provide additional evidence supporting the role of *CUL3* in ASD and/or ID with variable penetrance. Our study helps to identify and further define the clinical spectrum, including shared syndromic features among patients with LoF *CUL3* variants.

Methods

Identification of Pathogenic CUL3 Variants
We collected pathogenic variants in *CUL3* from exome, genome, or gene panel sequencing studies in patients through diagnostic clinical practice or institutional review board (IRB) approved research studies. Research subjects were also identified through GeneMatcher,[20] Deciphering Developmental Disorders (DDD) cohort,[21] and other professional communications. All variant coordinates are reported on GRCh37 (hg19) and transcript NM_003590.4.

Patient Consent and Ethics Declaration
The study was designed and initiated while P.R.B. was at the Mayo Clinic. Approval for the study was provided by the Mayo Clinic IRB (IRB 12-009346). F.E. performed functional investigations on human samples, which were approved by the ethics board of the Universitätsmedizin Greifswald (ethics no. BB 014/14). Patient informed consent for participation and phenotyping was obtained through each of the referring clinicians and centers. Clinical records including information related to neurodevelopmental, behavioral, dysmorphology, and other related phenotypic features were collected. Informed consent for the collection of patient blood samples and clinical information, including patient photos, was further obtained in accordance with the recognized standards of the Declaration of Helsinki and approved by local IRBs at the referring institutions.

Statistical Analyses
We collected 6 large exome and genome sequencing cohorts, excluding potential sample duplicates. For example, for cohorts including the DDD study, Autism Sequencing Consortium (ASC), and Radboud cohort, we only included the samples in their latest publication,[22] where potential duplicates have been removed as described in their study methodology. We also excluded all the Simons Simplex Collection (SSC) samples used in the ASC study[23] to avoid any potential redundancy with the SSC exomes.[15] We performed *de novo* enrichment analyses using 3 models: the chimpanzee-human (CH) divergence model, denovolyzeR, and DeNovoWEST. Each method applies its own underlying variant rate estimates to generate the prior probabilities for observing a specific number and class of variants for a given gene: (1) CH model estimates the number of expected *de novo* variants by incorporating locus-specific transition, transversion, and indel rates, as well as chimpanzee–human coding sequence divergence and gene length; (2) denovolyzeR estimates mutation rates based on trinucleotide context and incorporates exome depth, mutational biases such as CpG hotspots, and divergence adjustments based on macaque–human comparisons; and (3) DeNovoWEST scores all classes of coding variants on a unified severity scale based on the empirically estimated positive predictive value of being pathogenic. It incorporates a gene-based weighting derived from the deficit of protein-truncating variants in the general population and further combines missense enrichment by a clustering test. Default parameters were used for all 3 methods as described previously.[22,24] The expected mutation rate of 1.8 *de novo* variants per exome was set to the CH model as an upper bound baseline. The exome-wide significance cutoff ($p < 4.16E-07$) is determined after the Bonferroni multiple-testing correction considering both the ~20,000 genes in a human genome and the total of 6 tests per gene across the 3 models.

Patient Facial Analysis
We used GestaltMatcher[25,26] to measure the similarities of the facial phenotypes between individuals with variants in *CUL3*. The GestaltMatcher feature vectors derived from DeepGestalt[27] were used to span a 512-dimensional clinical face phenotype space (CFPS). Each image is a point located in CFPS, and the similarity between the 2 images was quantified by the cosine distance. In CFPS, the images with close distance were considered to have a high overlap of syndromic facial features. To further improve the performance and stability, we used test-time augmentation and model ensemble techniques.

We first performed the statistical analysis to quantify the overall similarity among the 13 available facial photos (P1, P2, P3, P19, P20, P22, P23, P24, P25, P28, P29, P30, and P31) and compared to the control distributions. A total of 1696 images of 1335 patients and 328 syndromes of the GestaltMatcher Database[28] (GMDB; https://db.gestaltmatcher.org) were used to derive control distributions of mean pairwise cosine distances in CFPS stemming from (1) patients with the same syndrome and (2) random patients with different syndromes. For each syndrome, 100 cohorts of random sample sizes were drawn, and the mean pairwise cosine distance of the patients was calculated. Only unique cohorts were used to construct the distribution of mean pairwise cosine distance of patients stemming from the same syndrome. Additionally, the same number of cohorts consisting of random patients was drawn and used to construct the distribution

of mean pairwise cosine distances of random patients stemming from different syndromes. Via a receiver operating characteristic curve analysis, a threshold to distinguish cohorts stemming from the same syndrome and random patients is derived by maximizing the Youden index (sensitivity+specificity−1). We applied this approach in a 5-fold cross-validation, and the validation fold was used to test the Youden index of the resulting threshold. Finally, the control distributions and the corresponding threshold with the highest Youden index on the validation fold were chosen.

To test whether patients from a given cohort share a common phenotype, their mean pairwise cosine distance is calculated and compared with the derived threshold. Because P19 and P20 are family members, and P24 and P25 are also family members, the distances between related individuals are discarded to avoid confounding. Additionally, 100 random subcohorts were drawn to estimate the uncertainty of the mean pairwise cosine distance. If a proportion of at least 50% of those mean pairwise cosine distances falls below the threshold, it is considered evidence for a shared phenotype within the cohort.

To further investigate the similarity among patients on the individual level, we performed the pairwise comparison analysis on 13 *CUL3* patients and compared them to 4306 images with 257 different disorders from GMDB to simulate the real-world scenario. For each test image of a *CUL3* patient, we performed the leave-one-out cross-validation by putting the rest of the 12 *CUL3* patients into the space with 4306 images and calculating the ranks of the 12 patients to the testing image.

Patient T Cells
Peripheral blood mononuclear cells (PBMCs) used in this study were isolated from whole blood from patients and the related healthy family members (father and/or mother of the proband) by PBMC spin medium gradient centrifugation (pluriSelect, Leipzig, Germany). The collected PBMCs were expanded in U-bottom 96-well plates using feeder cells in RPMI 1640 supplemented with 10% human AB serum (both purchased from PAN-Biotech, Aidenbach, Germany) with 150U/ml IL-2 (Miltenyi Biotec, Paris, France) and 1μg/μl L-PHA (Sigma, Saint-Quentin-Fallavier, France) following the procedure of Fonteneau et al.[29] After 3 to 4 weeks of culture, resting T cells were washed and frozen as dry pellets for further use.

Sodium Dodecyl-Sulfate Polyacrylamide Gel Electrophoresis and Western Blot Analysis
Cell pellets from resting T cells isolated from patients and related controls were subjected to protein extraction by resuspending them in equal amounts of standard radio-immunoprecipitation assay (RIPA) buffer (50mM

Tris pH 7.5, 150mM NaCl, 2mM EDTA, 1 mM N-ethylmaleimide, 10μM MG-132, 1% NP40, 0.1% sodium dodecyl-sulfate [SDS]) before separation by 10 or 12.5% SDS-polyacrylamide gel electrophoresis and subsequent transfer to polyvinylidene fluoride membranes (200 V for 1 hour). Primary antibodies used in this study include anti-pan-ubiquitin (DAKO, Les Ulis, France), anti-ubiquitin K48-linkages (Cell Signaling Technology, clone D9D5, Beverly, MA, USA), anti-CUL3 (Elabscience, E-AB-10263, Houstin, TX, USA), anti-cyclin E1 (Cell Signaling Technology, clone D7T3U), anti- cyclin-dependent kinase 2 (CDK2) (Cell Signaling Technology, clone 78B2), anti-cyclin A2 (Cell Signaling Technology, BF683), anti-4E-BP1 (Cell Signaling Technology, clone 53H11), and anti-GAPDH (Cell Signaling Technology, clone 14C10). Proteins were visualized using anti-mouse or rabbit horseradish peroxidase conjugated secondary antibodies (1/5000) and an enhanced chemiluminescence detection kit (ECL) (Bio-Rad, Marnes-la-Croquette, France). The Western blot chemiluminescent signals were quantified by densitometry (ImageJ) and the values of pan-ubiquitin modified proteins, K48-linked ubiquitin-protein conjugates, CUL3, cyclin E1, CDK2, cyclin A2, 4E-BP1 were normalized to those of GAPDH. Data are presented as mean (± standard error of the mean) of each of the investigated proteins to GAPDH ratios for the control and proband group, respectively, as indicated. Statistical significance was assessed by unpaired t-test (*$p < 0.05$, ***$p < 0.001$).

RNA Isolation, Reverse-Transcription and Polymerase Chain Reaction Analysis
Blood specimens were collected by using the PaxGene Blood RNA System (Qiagen, Les Ulis, France) to stabilize total RNA, which was subsequently isolated using the PaxGene Blood RNA kit (Qiagen) following the manufacturer's instructions. Total RNA (100–500ng) was subjected to reverse-transcription using the M-MLV reverse transcriptase from Promega and quantitative polymerase chain reaction (qPCR) was performed using the Premix Ex Taq (probe qPCR purchased from TaKaRa, Saint-Germain-en-Laye, France) in duplicates to determine the mRNA levels of each target gene using FAM-tagged TaqMan Gene Expression Assays (Thermo Fisher Scientific, Saint-Herblain, France). TaqMan probes used in this study for interferon-stimulated gene (ISG) quantification included *IFI27*, *IFI44L*, *IFIT1*, *ISG15*, *RSAD2*, and *SIGLEC1*. The cycle threshold (Ct) values for target genes were converted to values of relative expression using the relative quantification (RQ) method ($2^{-\Delta\Delta Ct}$). Target gene expression was calculated relative to Ct values for the *HPRT1* control housekeeping gene. A type I interferon

(IFN) score was calculated for each sample following the procedure of Rice et al.[30]

Results

Excess of De Novo Variants in CUL3 among a Large NDD Cohort

Among our recent collection of *de novo* variants from a large NDD cohort with 46,247 trios (15189 ASD and 31058 DD),[15,22,23,31–33] there are 3 *de novo* missense variants and 16 *de novo* LoF variants (including 10 frameshift, 3 stop-gain, 2 splice-donor, and 1 splice-acceptor) identified in *CUL3* (Tables S1 and S2). We performed a comprehensive *de novo* enrichment analysis across all *de novo* variants and genes among this collection, where 3 different statistical models were applied independently in parallel (CH model,[13,34] denovolyzeR,[35] and DeNovoWEST[22]). After Bonferroni correction, exome-wide significance was supported by all 3 models for excess of *de novo* variants in *CUL3* ($p = 4.60E-24$ in CH model, $p = 2.59E-17$ in denovolyzeR, $p = 6.8E-11$ in DeNovoWEST). Our observations are in line with the intolerant scores in gnomAD v2.1.1,[36] which show that *CUL3* is highly intolerant to both missense and LoF (truncating) variants, with a missense Z score of 4.75 (observed/expected ratio [o/e] = 0.35 [0.3–0.4]) and the probability of being LoF intolerant being 1 (o/e = 0.1 [0.05–0.23]). Those 2 lines of evidence together further strengthen the role of *CUL3* variants in NDD.

Molecular Findings in the Newly Described CUL3 Clinical Series

Via a multicenter collaboration, we collected 37 individuals with rare heterozygous variants in *CUL3* (Table S3), including 35 LoF variants (17 frameshift, 12 nonsense, and 6 with canonical splice site variants) and 2 missense variants. Of these, 24 are *de novo*, 9 are inherited, and inheritance was unknown for the remaining 4 individuals as DNA from both parents was unavailable. Parental inheritance was noted in families F7, F8, F11, F17, F18, F22, and F25 (Fig 1). Formal evaluations and clinical details are provided for P20 (mother of P19 in F18) and P25 (mother of P24 and P26 in F22). Limited clinical information was available for several reportedly affected parents (mother of P7 and P8 in F7; father of P12 in F11). The mother of P9 (F8) has reported learning difficulties, but was not considered to have ID. The mother of P18 (F17) was reported to have mild ID with some speech difficulties, but a full evaluation was not performed. Although the mother of P29 (F2) is reported to be unaffected, she has not received a formal evaluation in the clinical setting. Recurrent LoF variants were observed in multiple unrelated families. Specifically, p.Ser517Profs*23 had the highest incidence and was observed in 4 unrelated individuals (2 *de novo* and 2 inherited), and p.Leu165Ilefs*37 and p.Arg247* were each identified in 2 unrelated individuals (both are *de novo*).

CUL3 is highly conserved among orthologues from several species, and the residues affected by missense variation show a high degree of evolutionary conservation (p.Tyr58Cys in unrelated individuals, P4 and P5; conserved in baker's yeast, *Saccharomyces cerevisiae*) (Fig 1). These variants are predicted to be damaging by multiple tools (CADD, PolyPhen2, SIFT). Additionally, all variants are absent or extremely rare in the population (gnomAD v2.1.1) (Tables S3 and S4).[36] All 5 canonical splice site variants were predicted to result in donor loss and/or altered splicing of several exons and were notably absent from exon 9, which is affected in patients with pseudohypoaldosteronism type IIE (Fig 1, Table S5).

Three patients had secondary genetic findings of uncertain clinical significance, and their contribution to the overall clinical phenotype in these individuals is unclear. P2 carries a *de novo* nonsense variant (p.Tyr341*) in *CUL3* and a *de novo* missense variant in *CHD3* (NM_001005273.2, c.5863G>T, p.Ala1955Ser). The variant in *CHD3* was previously reported in Drivas et al,[37] falls near the end of the protein in an unannotated portion of the protein, and does not cluster with other disease-implicated missense variants in the conserved SNF2 family N-terminal or Helicase C-terminal domains. P31 has a *de novo* splice site variant (c.883+1G>T) in intron 6 of *CUL3*, together with a *de novo* missense variant (NM_001282948.1, c.6260A>C, p.Asp2087Ala) in *JMJD1C*. De novo heterozygous missense and LoF variants in *JMJD1C* have been implicated variably in patients with DD, ASD, and a phenotype resembling classical Rett syndrome.[38,39] P32 has a *de novo* frameshift variant (p.Ser517Profs*23) in *CUL3*, as well as a 22q12.3 duplication (arr 22q12.3 [33,421,825 − 34,080,737] × 3 pat) that includes a portion of the *LARGE* and *SYN3* genes, which was inherited from his apparently normal father. Overlapping duplications have been implicated in increased risk of ASD and other NDDs, however, the significance of this relatively small duplication is unclear.[40] To our knowledge, no other patients had secondary reportable alterations of clinical significance in this cohort.

Variants in CUL3 Define a Neurodevelopmental Syndrome

The 37 cases (23 males and 14 females) included in the study are from 33 families who carry heterozygous, mainly predicted LoF variants in *CUL3* through genome, exome, or custom gene panel sequencing. Affected individuals
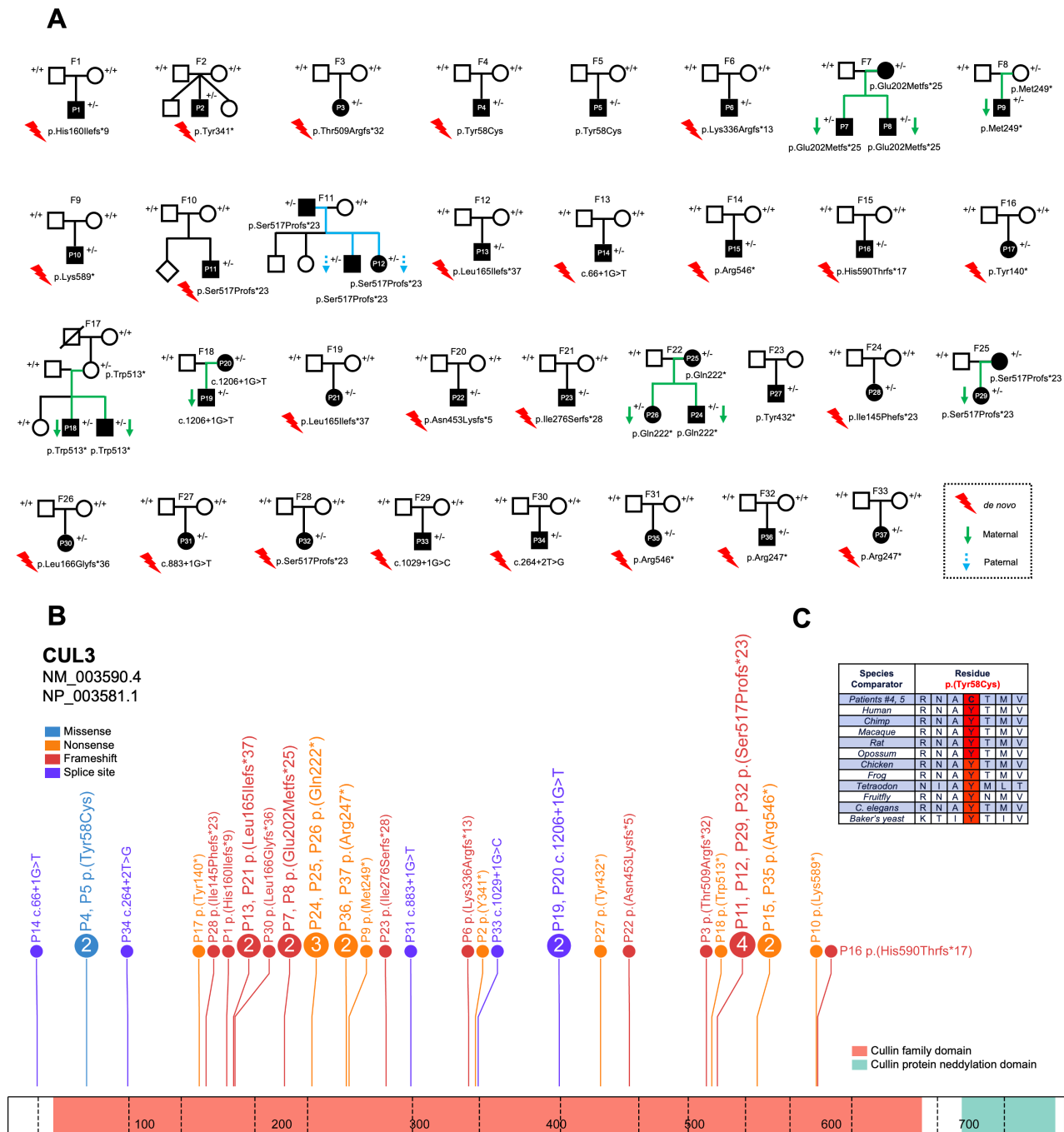
FIGURE 1: Samples in study. (A) Families and patients with index number included in study. Variants with a lightning bolt symbol (red) are *de novo*, maternally inherited variants are indicated with a solid arrow (green) and paternally inherited variants with dotted arrow (blue). (B) Variant distribution on the protein diagram of CUL3. (C) Amino acid conservation across species for the missense variant (p.Tyr58Cys) in P4 and P5.

presented with global DD (94%, 35/37), delayed speech and language development (97%, 34/35), dysmorphic facial features (high forehead, long face, and other variable features) (87.5%, 28/32) (Fig 2A), mild to severe ID (87%, 29/33), gross and fine motor delays (69%, 20/29 and 97%, 29/30, respectively), ASD (36%, 13/36), abnormalities of the hands and feet (51%, 18/35) (Fig 2B) (including bilateral 5th finger clinodactyly, thenar

hypoplasia, single palmar crease, ankle/foot contractures, pes cavus, cutaneous syndactyly second/third toes, hallux valgus etc.), and tremor and/or dystonia (20%, 7/35) (Tables S4 and S6).

Prenatal and Early Postnatal Presentation

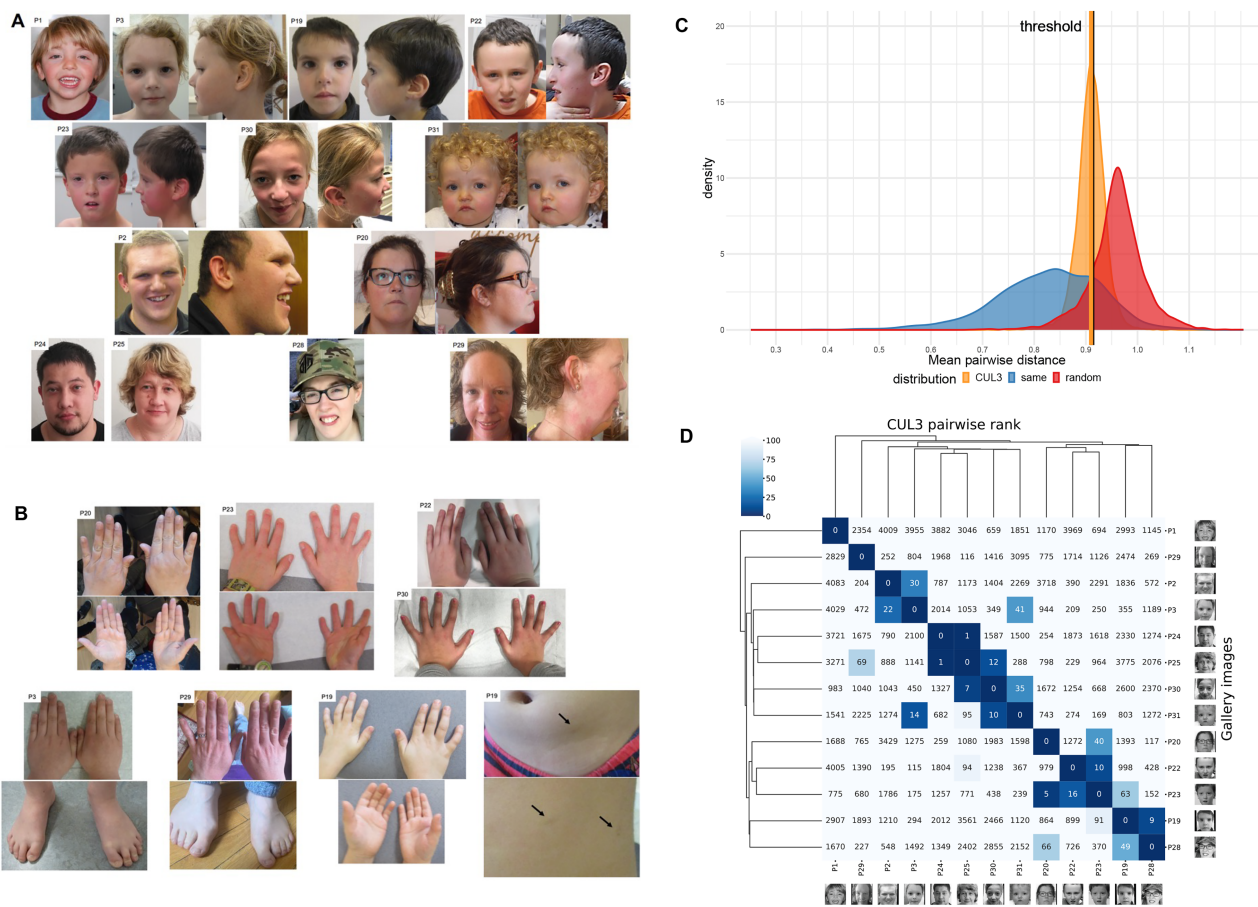Approximately 36% (13/36) of patients were found to have intrauterine growth restriction during gestation. Birth

FIGURE 2: The patient phenotype, distribution of mean pairwise distance, and the hierarchical clustering of facial photos. The phenotypic photos for available patients include front and profile facial images in (A) and images of hands and feet from individual patients in (B); P19 was noted to have several café-au-lait spots (*arrows*) on his abdomen and trunk. (C) It shows 3 distributions: *CUL3* (middle; *orange*), the random selection from the subjects with 328 disorders (right; *red*), and the selection with the same disorder (left; *blue*). 53.72% of the *CUL3* sampling with mean pairwise distance (0.9100) were below the threshold (0.9124; *blackline*). (D) Gallery images were the images in clinical face phenotype space (CFPS), which can be matched. Each column is the result of testing 1 subject in the column and listing the rank of the rest for the 12 photos in each row. For example, by testing P25, P30 was on the 7th rank and P23 was on the 5th rank of P20.

length, weight, and occipitofrontal circumference, when available, were variable but usually fell within the low-normal range (Table S4). Gastroesophageal reflux disease was noted in infancy in 31% (9/29) of subjects. Cleft palate was observed in 1 individual, and cryptorchidism was the most common genitourinary abnormality noted at birth (3 individuals).

Facial Features

As noted above, most individuals in the cohort were reported to have dysmorphic facial features, which were usually mild and were somewhat variable (Fig 2A). Several individuals were macrocephalic, with long triangular facies, including a large forehead and pointed chin. Ears were slightly dysplastic to normal and were small and posteriorly rotated in some individuals. The nose was bulbous in some with a wide nasal bridge. Some patients had a high arched palate and/or retrognathia. Eyes were deep

set with slightly narrow/downslanting palpebral fissures with epicanthal folds noted in some. Strabismus was noted in 4 individuals.

To further study defining facial features, we performed analyses with GestaltMatcher using individual photographs of the 13 patients for whom photographs were available. GestaltMatcher can be used to validate whether patients in a given cohort share a common phenotype. To do so, the mean pairwise cosine distance between patients of a cohort is analyzed. It was then compared to 2 control distributions of mean pairwise cosine distances stemming from (a) patients with the same syndrome and (b) random patients with different syndromes and a threshold (c) to distinguish cohorts stemming from (a) or (b) can be derived, resulting in c = 0.9124 with a corresponding sensitivity of 0.86 and a specificity of 0.79. For CUL3, we calculated the mean pairwise distance of 13 patients, whereas distances between related individuals

were discarded. This resulted in a mean pairwise cosine distance d = 0.9100 < c. Furthermore, 53.72% of mean pairwise cosine distances of sampled sub-cohorts fell below the threshold, indicating a moderate degree of similarity (Fig 2C). Overall, the analysis supports the hypothesis of a shared phenotype among *CUL3* patients.

To further investigate the similarity on the individual level, pairwise ranks analysis (Fig 2D) was performed. Most of the individuals showed significant similarity as expected. Seven pairs of subjects, (P2, P3), (P3, P31), (P19, P28), (P20, P23), (P22, P23), (P25, P30), and (P30, P31), were among the top-30 rank of each other in overall 4306 subjects. Moreover, P30 was at the 7th rank of P25, P23 was at the 5th rank of P20. Overall, combining the cohort and individual level analysis, the results showed a moderate degree of facial similarity, suggesting a recognizable pattern of facial dysmorphism. However, some pairs of patients might present with heterogeneous facial dysmorphic features (Fig 2D). Of note, previous studies have shown that DeepGestalt can be influenced by confounding factors such as age and ethnic background.[41,42] In the clustering dendrogram, the pair of P24 and P25 were at the 1st rank to each other. This may be due to confounding factors because they are family members. A more comprehensive analysis of the confounding effects is required when more photos are collected in the future.

Developmental Delay and Intellectual Disability

Speech delay was the most consistent feature and was noted in 97% (34/35). It was usually mild, but moderate to severe in 7 individuals. Some form of ID was noted in 87% of patients (29/33), although several patients were too young to assess. The severity of ID was again mild in most cases and moderate to severe in 9 cases. Formal intelligence quotient testing was performed in 8 individuals and ranged from 49 to 108 (median 62). Early hypotonia was seen in 50% of individuals (17/34), but improved or resolved with age in most individuals. There was a high degree of clinical suspicion for or a formal diagnosis of ASD in 36% of patients (13/36). Additional abnormalities and behavioral issues were noted in 57% of patients (16/28) and consisted of dysgraphia, slow information processing and spatial reasoning, agitation, (hetero-) aggressivity, impaired social interactions, poor frustration tolerance, and obsessive–compulsive disorder and repetitive behaviors. No consistent brain structural abnormalities were noted in the patient cohort. Most individuals who had a brain magnetic resonance imaging (MRI) performed had a normal study, but 3 were noted to have mild ventriculomegaly. Seizures, in contrast to previous studies, were observed in only a few patients and were either febrile

seizures or consisted of single isolated episodes suggesting that this may not be a recurrent clinical feature.

Dystonia and Movement Abnormalities

Movement abnormalities were noted in several patients (7/37 with noted tremor/spasm) in this cohort including 5 individuals with variable dystonia. P23 had *de novo* p.Ile276Serfs*28 alteration and developed tremor, myoclonus, and had severe motor delays. P24 and P26 both carried a maternally inherited variant (p.Gln222*); P24 had hyperreflexia, hand ataxia, cervical dystonia (onset at 23 years), truncal dystonia, and laryngeal dystonia (onset at 21 years), which led to speech problems. P26, the affected female sibling of P24, was diagnosed with diparetic form of cerebral palsy, with a history of congenital hydrocephalus, and temporal epilepsy. Their mother, P25, had hand tremor since childhood, which was not very progressive, adult onset oromandibular dystonia with speech involvement, and sudden recent onset of hyperreflexia. P28, with a *de novo* p.Ile145Phefs*23 alteration, had generalized dystonic body movements and spasms in her lower limbs (onset at age 27). Her episodes of muscle spasms were associated with shortness of breath, sweating, high blood pressure, and tachycardia. Finally, P30 (*de novo* p.Leu166Glyfs*36 alteration) developed facial hypotonia during infancy and later left inferior limb dystonia, with slow movements and an unusual gait marked by bilateral hip internal rotation. This appears to be a novel finding in this cohort of patients, and further study is warranted.

Hypertension and Other Cardiac Abnormalities

Several LoF mutations in *CUL3* have been reported in large trio exome studies of congenital heart disease.[11,43] One patient (proband 1–00577) with a *de novo* frameshift variant (p.Ile145Phefs*23) in *CUL3* was described with left ventricular obstruction, hypoplastic mitral valve, hypoplastic aortic annulus, aortic stenosis, coarctation, congenital hip dysplasia, and congenital scoliosis.[11] Another patient (proband 1-07184) with *de novo* stop-gain variant (p.Gln132*) had a left aortic arch with normal branching pattern, partially anomalous pulmonary veins, pulmonary valve stenosis, and sinus venosus septal defect, superior type.[43] In this study, we found 3 patients with various heart abnormalities: P1 with pulmonic stenosis and pulmonary valve dysplasia, P17 with a ventricular septal defect, and P24 with mild mitral valve insufficiency (ejection fraction 55%, cardiac MRI normal). Two patients presented with conduction defects including 1 with sinus rhythm with short PR interval and nonspecific T wave abnormalities, and 1 with sinus rhythm and supraventricular and rare ventricular extrasystoles. Five patients

presented with unexplained early onset/juvenile hypertension in the absence of hyperkalemia.

CUL3 Variants Are Associated with Ubiquitin Conjugation Deficiency and Accumulation of CUL3 Substrates in Patient Cells

Because CUL3 serves as a scaffolding subunit of an E3 ubiquitin ligase complex supporting the ubiquitination of several substrates,[44] we next evaluated the functional consequences of the identified *CUL3* alterations on the ubiquitin-conjugation system in patient cells. In total, T cells were isolated from 10 individuals carrying 8 *CUL3* variants: p.Tyr58Cys (P4 and P5), p.Ser517Profs*23 (in 4 unrelated individuals [P11, P12, P29, and P32]), p.-Trp513* (proband P18 and his unaffected mother),

c.1206+1G>T (proband P19 and his mother P20), p.-Tyr341* (P4), c.66+1G>T (P14), p.Leu166Glyfs*36 (P30), and c.883+1G>T (P31), which were assessed for their content in ubiquitin-modified proteins by Western blotting using an anti-pan ubiquitin antibody. The amounts of ubiquitin-protein conjugates were substantially reduced in all investigated patients when compared to those from 6 healthy related or unrelated donor controls (Fig 3A, D). Probing the membrane with an antibody specific for ubiquitin K48 linkages revealed a similar pattern (Fig 3B, D), indicating that patients failed to assemble ubiquitin chains for the modification of substrates destined for proteasomal degradation. Importantly, the decreased ubiquitination detected in patients with *CUL3* alterations was accompanied by a decreased
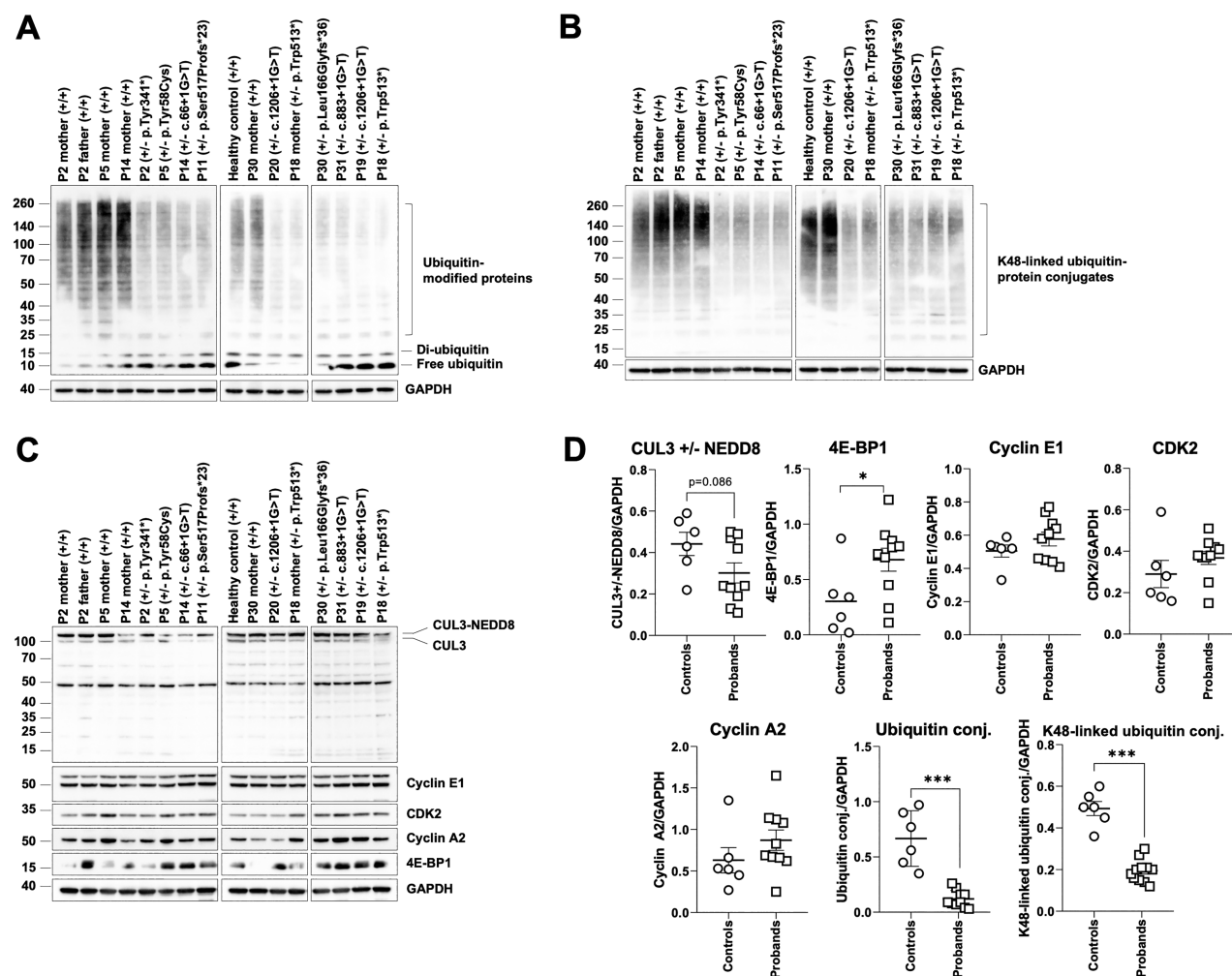

FIGURE 3: Cells isolated from subjects carrying *CUL3* variants exhibit signs of ubiquitin homeostasis perturbations resulting in the stabilization of CUL3 substrates. Five to 40μg of radioimmunoprecipitation assay lysates from T cells isolated from *CUL3* patients and control samples were separated by sodium dodecyl-sulfate-polyacrylamide gel electrophoresis followed by Western blotting using antibodies directed against pan-ubiquitin modified proteins (A), K48-linked ubiquitin-modified proteins (B) as well as CUL3, cyclin E1, cyclin-dependent kinase 2 (CDK2), cyclin A2, 4E-BP1 (C), as indicated. Equal protein loading was ensured by probing the membranes with an anti-GAPDH antibody. Western blot densitometry analysis (D) was performed and the values of pan-ubiquitin modified proteins, K48-linked ubiquitin-modified proteins, CUL3, cyclin E1, CDK2, cyclin A2, 4E-BP1 were normalized to those of GAPDH.

steady state expression of both free and NEDD8-bound CUL3 full-length proteins in most patients, as determined by Western blotting. The reduction in CUL3 levels was particularly pronounced in P2, P5, P14, P11, P19, and P18 (Fig 3C, D), indicating that this phenomenon was not associated with a specific variant type. Of note, we could not detect the truncated variants, p.Ser517Profs*23, p.Trp513*, p.Tyr341*, p.His160Ilefs*9, or p.Leu166Glyfs*36 with a predicted size of 63, 60, 40, 20, and 16 kDa, respectively. Likewise, our anti-CUL3 antibody failed to detect any truncated CUL3 or aberrantly spliced species emerging from the c.1206+1G>T, c.66+1G>T, or c.883+1G>T alterations.

Because CUL3 has been shown to target cyclin E1 and 4E-BP1 for degradation,[45,46] we next examined the expression level of both proteins in patient cells. Although a significant stabilization of 4E-BP1 was detected in nearly all patient-derived T cells, a slight upregulation of cyclin E1 was detected only in P14, P11, P31, P19, and P18 (Fig 3C, D). This upregulation was accompanied by stabilization of a cyclin E1 binding partner, CDK2, in these same probands (Fig 3C, D). These findings suggest that, depending on the variant, there is a partial impairment in *CUL3*'s ability to ubiquitinate and target its substrates for proteasomal degradation. Taken together, these data point to a clear role of *CUL3* LoF variants in patient cells impacting the protein turnover of several components of the cell cycle and translational machinery.

CUL3 *LoF Variants Do Not Promote a Type I IFN Signature*

Because proteasome LoF variants typically associated with the generation of a sterile type I IFN response in patients with proteasome-associated autoinflammatory syndromes (PRAAS),[47–53] we next attempted to clarify whether *CUL3* variants generate such a signature as well. To address this, we compared the expression of 6 IFN-stimulated genes (ie, *IFI27*, *IFI44L*, *IFIT1*, *ISG15*, *RSAD2*, and *SIGLEC1*) in PAXgene blood RNA samples from patients and controls. Although ISG15 was constitutively induced in 7 of 10 probands investigated (Fig S1), our data revealed that the IFN scores did not substantially differ between patients and controls. These findings also indicate that *CUL3* LoF variants, despite disrupting ubiquitin homeostasis of several known targets, do not promote a type I IFN gene signature (Fig 4 and Fig S1).

Discussion

In this study, we defined the phenotypic spectrum in 37 individuals carrying rare heterozygous variants in *CUL3*. Except 2 patients with a recurrent missense variant
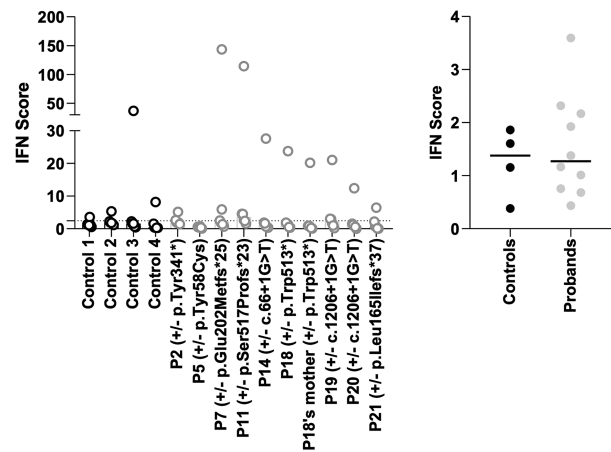

FIGURE 4: Subjects carrying *CUL3* variants do not spontaneously initiate sterile type I interferon (IFN) responses. IFN scores for the controls and *CUL3* subjects were calculated as the median of the relative quantification (RQ) of the 6 interferon-stimulated genes (ISGs) *IFIT1*, *IFI27*, *IFI44L*, *ISG15*, *RSAD2*, and *SIGLEC1* over a single calibrator control. Shown are the IFN scores of each sample (*left panel*) and the sample groups (ie, controls and *CUL3* subjects) as indicated (*right panel*).

observed in a highly conserved residue, the vast majority are frameshift, nonsense, or canonical splice site variants that are predicted to result in *CUL3* haploinsufficiency. The clinical manifestation, although variable, has a number of consistent findings including DD and ID in the vast majority of patients. Behavioral difficulties were also very prevalent with a subset diagnosed with ASD. Learning difficulties were most often accompanied with speech delay and other processing issues and ranged in severity from mild to profound. Patients also presented with both gross and fine motor delays early in development. A subset of patients presented with early hypotonia, which resolved over time. A smaller group of patients developed later (usually adult) onset dystonia and tremor. However, epilepsy, which was thought to be a part of the clinical spectrum, was not observed in our patient cohort (OMIM 619239).

Several recurrent facial features were noted in our cohort including relative macrocephaly and a long triangular face with a prominent forehead and pointed chin (Fig 2A). Ears were normal appearing in most individuals, but were small, dysplastic, and posteriorly rotated in some. Several individuals had a bulbous nose with a wide nasal bridge. Eyes were described as deep set with slightly narrow/downslanting palpebral fissures with epicanthal folds noted in several individuals. We performed facial analysis on 13 individuals with available frontal photos using GestaltMatcher, which identified several similarities among unrelated individuals in our cohort (Fig 2C). In summary, most of the available subjects with *CUL3* variants presented

11

with similar facial dysmorphisms. However, only 13 of 37 individuals consented to the facial analysis. A comprehensive analysis with more photos to exclude possible confounding effects is required in the future.

CUL3 is expressed in a variety of different tissues including brain and nerve tissue, but has the highest expression levels in testis, skeletal muscle, heart, esophagus mucosa, skin, and the uterus (based on GTEx data accessed on June 30, 2024). We identified several clinical phenotypes affecting these tissues, suggesting that *CUL3* haploinsufficiency may influence expression of some of these traits. For instance, although the role of gain-of-function splice variants affecting exon 9 of *CUL3* is well known in renal hyperkalemia and hypertension in autosomal dominant pseudohypoaldosteronism, type IIE (OMIM 614496), we identified several individuals in our cohort without electrolyte abnormalities who had early or juvenile onset hypertension or other congenital cardiac abnormalities. A few patients were noted to have abnormal (thickened) scarring, delayed wound healing, or easy bruising. One patient (P13) was noted to have cutaneous dyschromia (Fig 2B). Although relatively nonspecific, several patients had gastroesophageal reflux disease in infancy and early childhood. Several additional congenital anomalies were noted, including abnormalities of the hands and feet (53%, 17/35) (Fig 2B), most notably bilateral 5th finger clinodactyly in 4 individuals, thin thumbs and thenar hypoplasia in 2 individuals, single palmar crease in 3 individuals, contractures involving the ankles, feet, or toes in 5 (talipes equinovarus in 1 individual), pes cavus in 5 individuals, cutaneous syndactyly second/third toes in 2 individuals, and hallux valgus in 2 individuals. Several patients were noted to have scoliosis or severe lordosis. Oscillating testis, retractile testis, and cryptorchidism noted in 1 patient each. Overall, the appearance of several recurrent clinical phenotypes in our cohort implicates *CUL3* in a syndromic ID/ASD disorder.

Functional studies showed that subjects harboring *CUL3* variants show dysfunction of the ubiquitin-proteasome system (UPS), as evidenced by their decreased content of ubiquitin-protein conjugates (Fig 3A, B). Such reduced amounts of ubiquitin-modified proteins might reflect a general ubiquitin-conjugation deficiency in these patients, as a consequence of loss of function for CUL3. In line with this assumption, 4E-BP1 and, to a lesser extent, cyclin E1, 2 prominent substrates of CUL3, failed to be targeted for proteasomal degradation in most investigated subjects (Fig 3C). The inefficiency of CUL3 to ubiquitinate its intracellular target proteins in patients might be because of insufficient expression levels, as evidenced by lower protein levels in mutant compared to control cells for most variants. Importantly, we were unable to detect any of the CUL3 truncated variants potentially resulting from the tested nonsense, frameshift, or splicing alterations. One potential explanation for this result may be the specificity of our anti-CUL3 antibody, which may be exclusively directed to the C-terminal part of the protein and, as such, unable to recognize C-terminal truncated variants. Alternatively, it is also conceivable that such variants may be degraded by nonsense-mediated mRNA decay and therefore not subjected to translation. In any case, this issue warrants further investigation. The abnormal accumulation of cyclin E1 and its binding partner CDK2 in patients with *CUL3* variants (Fig 3C) may actively contribute to the pathogenesis of the observed neurodevelopmental delay. Overexpression of cyclin E1 in embryonic murine brains has been associated with dysregulation of corticogenesis.[54] Likewise, stabilized 4E-BP1 may be implicated in the neuronal phenotype by impeding protein translation.

Our data show that, unlike in proteasomal disruption, *CUL3* LoF is not associated with a type I IFN gene signature (Figs. 4 and S1). These data are interesting and suggest that the generation of such signature clearly depends on the type of ubiquitin homeostasis imbalance with which the cells are confronted. Hence, any shift toward accumulation of ubiquitin-modified proteins promotes a type I IFN response, although any change toward deficiency would not necessarily result in autoinflammation. Our report is currently the most comprehensive phenotypic analysis of patients with rare heterozygous mainly LoF variants in *CUL3*. Our cohort analysis suggests that *CUL3* haploinsufficiency is associated with a disorder characterized by ID with or without autistic features, variable congenital anomalies, and facial dysmorphisms, which together constitute a clinically recognizable syndrome. Our study also provides strong evidence supporting the role of CUL3 as a member of an emerging group of cullinopathies, which has wide-ranging effects on development, but its mechanism is still being elucidated.

Acknowledgement

Materials according to the journal policy. We sincerely appreciate all the families who participated in this study. We thank T. Brown for assistance in editing this manuscript, and A. Brandenburg for excellent technical assistance.

Author Contributions

Potential Conflicts of Interest

Nothing to report.

Data Availability

All of the patient variant and phenotype data used in this study has been provided in the supplementary tables.

References

1. Sarikas A, Hartmann T, Pan Z-Q. The cullin protein family. Genome Biol 2011;12:220.

2. Baek K, Scott DC, Schulman BA. NEDD8 and ubiquitin ligation by cullin-RING E3 ligases. Curr Opin Struc Biol 2021;67:101–109.

3. Zou Y, Liu Q, Chen B, et al. Mutation in CUL4B, which encodes a member of Cullin-RING ubiquitin ligase complex, causes X-linked mental retardation. Am J Hum Genetics 2007;80:561–566.

4. Tarpey PS, Raymond FL, O'Meara S, et al. Mutations in CUL4B, which encodes a ubiquitin E3 ligase subunit, cause an X-linked mental retardation syndrome associated with aggressive outbursts, seizures, relative macrocephaly, central obesity, hypogonadism, pes Cavus, and tremor. Am J Hum Genetics 2007;80:345–352.

5. Huber C, Dias-Santagata D, Glaser A, et al. Identification of mutations in CUL7 in 3-M syndrome. Nat Genet 2005;37:1119–1124.

6. Boyden LM, Choi M, Choate KA, et al. Mutations in kelch-like 3 and cullin 3 cause hypertension and electrolyte abnormalities. Nature 2012;482:98–102.

7. Nakashima M, Kato M, Matsukura M, et al. De novo variants in CUL3 are associated with global developmental delays with or without infantile spasms. J Hum Genet 2020;65:727–734.

8. Kato K, Miya F, Oka Y, et al. A novel missense variant in CUL3 shows altered binding ability to BTB-adaptor proteins leading to diverse phenotypes of CUL3-related disorders. J Hum Genet 2021;66: 491–498.

9. Iwafuchi S, Kikuchi A, Endo W, et al. A novel stop-gain CUL3 mutation in a Japanese patient with autism spectrum disorder. Brain Dev 2020;43:303–307.

10. Vincent KM, Bourque DK. A novel splice site CUL3 variant in a patient with neurodevelopmental delay. Brain Dev 2023;45:244–249.

11. Zaidi S, Choi M, Wakimoto H, et al. De novo mutations in histone-modifying genes in congenital heart disease. Nature 2013;498: 220–223.

12. Kong A, Frigge ML, Masson G, et al. Rate of de novo mutations and the importance of father's age to disease risk. Nature 2012;488: 471–475.

13. O'Roak BJ, Vives L, Girirajan S, et al. Sporadic autism exomes reveal a highly interconnected protein network of de novo mutations. Nature 2012;485:246–250.

14. Wang T, Guo H, Xiong B, et al. De novo genic mutations among a Chinese autism spectrum disorder cohort. Nat Commun 2016;7: 13316.

15. Study TD, Autism HMC. For, consortium U, et al. Synaptic, transcriptional and chromatin genes disrupted in autism. Nature 2014;515: 209–215.

16. Kosmicki JA, Samocha KE, Howrigan DP, et al. Refining the role of de novo protein-truncating variants in neurodevelopmental disorders by using population reference samples. Nat Genet 2017;49: 504–510.

17. Lin GN, Corominas R, Lemmens I, et al. Spatiotemporal 16p11.2 protein network implicates cortical late mid-fetal brain development and KCTD13-Cul3-RhoA pathway in psychiatric diseases. Neuron 2015; 85:742–754.

18. Dong Z, Chen W, Chen C, et al. CUL3 deficiency causes social deficits and anxiety-like behaviors by impairing excitation-inhibition balance through the promotion of cap-dependent translation. Neuron 2019;105:475–490.e6.

19. Morandell J, Schwarz LA, Basilico B, et al. Cul3 regulates cytoskeleton protein homeostasis and cell migration during a critical window of brain development. Nat Commun 2021;12:3058.

20. Sobreira N, Schiettecatte F, Valle D, Hamosh A. GeneMatcher: a matching tool for connecting investigators with an interest in the same gene. Hum Mutat 2015;36:928–930.

21. Firth HV, Richards SM, Bevan AP, et al. DECIPHER: database of chromosomal imbalance and phenotype in humans using Ensembl resources. Am J Hum Genetics 2009;84:524–533.

22. Kaplanis J, Samocha KE, Wiel L, et al. Evidence for 28 genetic disorders discovered by combining healthcare and research data. Nature 2020;586:757–762.

23. Satterstrom FK, Kosmicki JA, Wang J, et al. Large-scale exome sequencing Study implicates both developmental and functional changes in the neurobiology of autism. Cell 2020;180:568–584.e23.

24. Wang T, Hoekzema K, Vecchio D, et al. Large-scale targeted sequencing identifies risk genes for neurodevelopmental disorders. Nat Commun 2020;11:4932.

25. Hsieh T-C, Bar-Haim A, Moosa S, et al. GestaltMatcher facilitates rare disease matching using facial phenotype descriptors. Nat Genet 2022;54:349–357.

26. Hustinx A, Hellmann F, Sumer O, et al. *Improving deep facial phenotyping for ultra-rare disorder verification using model ensembles. IEEE/CVF Winter Conference on Applications of Computer Vision (WACV) (IEEE, 2023)*, 2023. doi:10.1109/wacv56688.2023. 00499

27. Gurovich Y, Hanani Y, Bar O, et al. Identifying facial phenotypes of genetic disorders using deep learning. Nat Med 2019;25:60–64.

28. Lesmann H, Lyon GJ, Caro P, et al. GestaltMatcher Database—A global reference for facial phenotypic variability in rare human diseases [Internet]. medRxiv, 2024. Available from. https://www.medrxiv.org/content/10.1101/2023.06.06.23290887v3.

29. Fonteneau J-F, Larsson M, Somersan S, et al. Generation of high quantities of viral and tumor-specific human CD4+ and CD8+ T-cell clones using peptide pulsed mature dendritic cells. J Immunol Methods 2001;258:111–126.

30. Rice GI, Melki I, Frémond M-L, et al. Assessment of type I interferon signaling in pediatric inflammatory disease. J Clin Immunol 2017;37: 123–132.

31. Feliciano P, Zhou X, Astrovskaya I, et al. Exome sequencing of 457 autism families recruited online provides evidence for autism risk genes. Npj Genom Med 2019;4:19.

32. Yuen RKC, Merico D, Bookman M, et al. Whole genome sequencing resource identifies 18 new candidate genes for autism spectrum disorder. Nat Neurosci 2017;20:602–611.

33. Consortium TS, Feliciano P, Daniels AM, et al. SPARK: a US cohort of 50,000 families to accelerate autism research. Neuron 2018;97: 488–493.

34. Coe BP, Stessman HAF, Sulovari A, et al. Neurodevelopmental disease genes implicated by *de novo* mutation and copy number variation morbidity. Nat Genet 2019;51:106–116.

35. Ware JS, Samocha KE, Homsy J, Daly MJ. Interpreting *de novo* variation in human disease using denovolyzeR. Curr Protoc Hum Genetics 2015;87:7.25.1–7.25.15.

36. Karczewski KJ, Francioli LC, Tiao G, et al. The mutational constraint spectrum quantified from variation in 141,456 humans. Nature 2020; 581:434–443.

37. Drivas TG, Li D, Nair D, et al. A second cohort of CHD3 patients expands the molecular mechanisms known to cause Snijders Blok-Campeau syndrome. Eur J Hum Genet 2020;28:1422–1431.

38. Sáez MA, Fernández-Rodríguez J, Moutinho C, et al. Mutations in JMJD1C are involved in Rett syndrome and intellectual disability. Genet Med 2016;18:378–385.

39. Slavotinek A, Hagen JM v, Kalsner L, et al. Jumonji domain containing 1C (JMJD1C) sequence variants in seven patients with autism spectrum disorder, intellectual disability and seizures. Eur J Med Genet 2020;63:103850.

40. Sarasua SM, Dwivedi A, Boccuto L, et al. 22q13.2q13.32 genomic regions associated with severity of speech delay, developmental delay, and physical features in Phelan–McDermid syndrome. Genet Med 2014;16:318–328.

41. Lumaka A, Cosemans N, Mampasi AL, et al. Facial dysmorphism is influenced by ethnic background of the patient and of the evaluator. Clin Genet 2017;92:166–171.

42. Pantel JT, Zhao M, Mensah MA, et al. Advances in computer-assisted syndrome recognition by the example of inborn errors of metabolism. J Inherit Metab Dis 2018;41:533–539.

43. Jin SC, Homsy J, Zaidi S, et al. Contribution of rare inherited and *de novo* variants in 2,871 congenital heart disease probands. Nat Genet 2017;49:1593–1601.

44. Jerabkova K, Sumara I. Cullin 3, a cellular scripter of the non-proteolytic ubiquitin code. Semin Cell Dev Biol 2018;93:100–110.

45. Davidge B, Rebola KG d O, Agbor LN, et al. Cul3 regulates cyclin E1 protein abundance via a degron located within the N-terminal region of cyclin E. J Cell Sci 2019;132:jcs233049.

46. Yanagiya A, Suyama E, Adachi H, et al. Translational homeostasis via the mRNA cap-binding protein, eIF4E. Mol Cell 2012;46:847–858.

47. Arima K, Kinoshita A, Mishima H, et al. Proteasome assembly defect due to a proteasome subunit beta type 8 (PSMB8) mutation causes the autoinflammatory disorder, Nakajo-Nishimura syndrome. Proc National Acad Sci U S A 2011;108:14914–14919.

48. Kitamura A, Maekawa Y, Uehara H, et al. A mutation in the immunoproteasome subunit PSMB8 causes autoinflammation and lipodystrophy in humans. J Clin Invest 2011;121:4150–4160.

49. Liu Y, Ramot Y, Torrelo A, et al. Mutations in proteasome subunit β type 8 cause chronic atypical neutrophilic dermatosis with lipodystrophy and elevated temperature with evidence of genetic and phenotypic heterogeneity. Arthritis Rheum 2012;64:895–907.

50. Brehm A, Liu Y, Sheikh A, et al. Additive loss-of-function proteasome subunit mutations in CANDLE/PRAAS patients promote type I IFN production. J Clin Invest 2015;125:4196–4211.

51. Poli MC, Ebstein F, Nicholas SK, et al. Heterozygous truncating variants in POMP escape nonsense-mediated decay and cause a unique immune dysregulatory syndrome. Am J Hum Genetics 2018;102: 1126–1142.

52. de Jesus AA, Brehm A, VanTries R, et al. Novel proteasome assembly chaperone mutations in PSMG2/PAC2, cause the autoinflammatory interferonopathy, CANDLE/PRAAS4. J Allergy Clin Immun 2019;143:1939–1943.e8.

53. Sarrabay G, Méchin D, Salhi A, et al. PSMB10, the last immunoproteasome gene missing for PRAAS. J Allergy Clin Immun 2019;145:1015–1017.e6.

54. Pilaz L-J, Patti D, Marcy G, et al. Forced G1-phase reduction alters mode of division, neuron number, and laminar phenotype in the cerebral cortex. Proc National Acad Sci 2009;106:21924–21929.